Journal of Environmental Radioactivity 277 (2024) 107451

Contents lists available at ScienceDirect

Journal of Environmental Radioactivity

journal homepage: www.elsevier.com/locate/jenvrad

Effect of grain size variation on strontium sorption to heterogeneous aquifer sediments

Georgia R. Barker [a], Landis Jared West [a], James T. Graham [b], Liam Abrahamsen-Mills [c], Ian T. Burke [a,*]

[a] University of Leeds, UK
[b] National Nuclear Laboratory Ltd., Sellafield, CA20 1PG, UK
[c] National Nuclear Laboratory Ltd., Warrington, WA3 6AE, UK

ARTICLE INFO

Handling editor: S.C. Sheppard

Keywords:
Strontium-90
Sorption
Sediments cation exchange
Ionic strength

ABSTRACT

Strontium-90 (^{90}Sr) is a major contaminant at nuclear legacy sites. The mobility of ^{90}Sr is primarily governed by sorption reactions with sediments controlled by high surface area phases such as clay and iron oxides. Sr^{2+} adsorption was investigated in heterogeneous unconsolidated aquifer sediments, analogous to those underlying the UK Sellafield nuclear site, with grainsizes ranging from gravels to clays. Batch sorption tests showed that a linear K_d adsorption model was applicable to all grainsize fractions up to equilibrium [Sr] of 0.28 mmol L^{-1}. Sr^{2+} sorption values (K_d; Langmuir q_{max}) correlated well with bulk sediment properties such as cation exchange capacity and surface area. Electron microscopy showed that heterogeneous sediments contained porous sandstone clasts with clay minerals (i.e. chlorite) providing an additional adsorption capacity. Therefore, gravel corrections that assumed that the > 2 mm fractions are inert were not appropriate and underestimated $K_{d\ (bulk)}$ adsorption coefficients. However, $K_{d\ (<2\ mm)}$ values measured from sieved sediment fractions, were effectively adjusted to within error of $K_{d\ (bulk)}$ using a surface area dependant gravel correction based on particle size distribution data. Amphoteric pH dependent Sr^{2+} sorption behaviour observed in batch experiments was consistent with cation exchange modelling between pH 2–7 derived from the measured cation exchange capacities. Above pH 7 model fits were improved by invoking a coupled cation exchange/surface complexation which allowed for addition sorption to iron oxide phases. The overall trends in Sr^{2+} sorption (at pH 6.5–7) produced by increasing solution ionic strength was also reproduced in cation exchange models. Overall, the results showed that Sr^{2+} sorption to heterogeneous sediment units could be estimated from $K_{d\ (<2\ mm)}$ data using appropriate gravel corrections, and effectively modelled using coupled cation exchange and surface complexation processes.

1. Introduction

Strontium-90 (0.55 MeV; t½ = 28.8 years) is a major groundwater contaminant at nuclear sites worldwide, including Hanford (US), Mayak (Russia), Chernobyl (Ukraine) and Sellafield (UK) (Beresford et al., 2020; McKinley et al., 2007; Sellafield Ltd, 2016; Standring et al., 2002). The UK Sellafield nuclear site has the largest contaminated land liability in the Nuclear Decommissioning Authority's (NDA) estate (Cruickshank, 2012). Leaks to ground from waste storage ponds and tanks (such as Magnox Swarf Storage Silos, MSSS (Wallace et al., 2012)) have produced plumes of ^{90}Sr contaminated groundwater, and the potential mobility of ^{90}Sr from historical releases is now a significant risk to site decommissioning (Turkington et al., 2018).

^{90}Sr occurs in groundwater as $^{90}Sr^{2+}$ and its mobility is primarily controlled by adsorption to negatively charged mineral surfaces present in aquifer sediments (O'Day et al., 2000; Patterson and Spoel, 1981). Highly adsorbing phases include aluminosilicate clays (such as chlorite, montmorillonite) and Fe oxides (Carroll et al., 2008; Dyer et al., 2000; Trivedi and Axe, 1999). Incorporation into carbonate phases occurs under high pH conditions and at higher Sr^{2+} concentration, $SrCO_3$ precipitates (Hodkin et al., 2018). Most commonly, Sr^{2+} adsorbs to mineral surfaces by forming outer sphere complexes at the solid-water interface with ion exchange as the main mechanism (Fuller et al., 2016).

Therefore, sorption of Sr^{2+} in most soils and sediments is strongly

* Corresponding author.
E-mail addresses: eegrb@leeds.ac.uk (G.R. Barker), L.J.West@leeds.ac.uk (L.J. West), james.graham@uknnl.com (J.T. Graham), liam.abrahamsen-mills@uknnl.com (L. Abrahamsen-Mills), i.t.burke@leeds.ac.uk (I.T. Burke).

https://doi.org/10.1016/j.jenvrad.2024.107451
Received 27 March 2024; Received in revised form 9 May 2024; Accepted 13 May 2024
Available online 7 June 2024

affected by pH and ionic strength (Thorpe et al., 2012; Wallace et al., 2012), with either low pH or higher ionic strength leading to lower Sr^{2+} sorption (Krauskopf and Bird, 1967; Livens and Baxter, 1988; O'Day et al., 2000).

The background Sellafield groundwater environment is characterised by low ionic strength, circumneutral pH (pH 6–8) and oxidising conditions (Newsome et al., 2014; Sellafield Ltd, 2016; Thorpe et al., 2012), which are favourable for rapid sorption of Sr^{2+} to clay and iron oxide minerals present in aquifer sediments (McKenzie and Armstrong-Pope, 2010; Sellafield Ltd, 2016). However, historical accidental leaks from radionuclide storage tanks have increased the ionic strength within contaminant plumes (Wallace et al., 2012). Sellafield, like many other UK nuclear sites, lie on coastal plains which have been identified as vulnerable to saline water intrusion from sea level rise (Chang et al., 2018) potentially affecting ^{90}Sr sorption (Eagling et al., 2013).

A simple distribution function between the aqueous and solid phases present (K_d) has been measured under a range of scenarios to characterise the chemical interaction between ^{90}Sr and sediment surfaces (Axe et al., 1998; Fuller et al., 2016). K_d values are used to calculate retardation factors (Rf) commonly used by contaminant modellers to predict fate and transport of ^{90}Sr (Appelo and Postma, 2004). The standardised method of measuring K_d involves sieving the sample to <2 mm, which produces a result skewed to fine grained, high surface area phases such as clays or iron oxides. Since the >2 mm sediment fraction has a low surface area to volume ratio, it has relatively low adsorption capacity (Langmuir, 1997). Common practise for heterogeneous sediments, therefore, assumes that >2 mm particles are inert. Where a large >2 mm fraction is present, gravel corrections can be applied to account for either an inert gravel fraction or one with a lower K_d than the < 2 mm fraction (Um et al., 2009). Using gravelly sediments from the US Hanford nuclear site, an empirical method was developed to calculate gravel corrected Sr K_d values (Kaplan et al., 2000).

The complex subsurface underlying the Sellafield nuclear site is characterised by Quaternary glacial outwash sediments with grainsizes ranging from clay to gravel. Borehole records showed gravel and sand channels interspersed by clay and silt lenses (Smith et al., 2020, 2023). Unconsolidated coarse grained gravel layers provide preferential pathways for groundwater flow and therefore play an important role in rapid contaminant transport. Although remediation strategies for U(VI) contamination (via bioreduction) have been assessed using the gravel fraction (Newsome et al., 2014), investigations of ^{90}Sr adsorption behaviour has relied exclusively on characterisation of the <2 mm fraction (Fuller et al., 2016; Small et al., 1999; Thorpe et al., 2012; Wallace et al., 2012). Therefore, there is a lack of directly measured Sr^{2+} adsorption data for the full range of grainsizes relevant to the UK Sellafield nuclear site. In addition, the fate of ^{90}Sr adsorbed to coarse sediments has not been assessed as a function of geochemical conditions including pH and ionic strength.

Therefore, our study aimed to characterise the geochemistry of >2 mm fraction to determine its effect on K_d values. The specific objectives are to improve understanding of Sr^{2+} adsorption behaviour as a function of grainsize and assess existing methods used to quantify Sr adsorption in a range of heterogeneous aquifer sediments, relevant to the UK Sellafield nuclear site (including the 2–22 mm fractions) using batch sorption tests. The effect of changing groundwater pH and ionic strength is also determined. This new information better informs K_d parameterisation for future assessment modelling of ^{90}Sr contaminant transport through heterogeneous glacial sediments, leading to more robust estimates of risk and contaminated land volumes.

2. Materials and methods

2.1. Sediment sampling

Five 25 kg samples of fluvioglacial alluvium deposits (A-E, representing a range of grainsizes present at this location) were collected from an exposed cliff section at Drigg Beach, Cumbria in April 2021 (54° 22′ 31.5″ N, 3° 28′ 16.4″ W). This exposed section is representative of the same unconsolidated sediment facies that underlies the Sellafield nuclear legacy site UK, composed of 0–60 m of Quaternary fluvioglacial deposits consisting of sand and gravel channels with clay and silt lenses (Smith et al., 2020, 2023). At the Sellafield site, sediments are water saturated from 9 to 10 m below the surface and groundwater levels vary seasonally by only ±1 m (Kuras et al., 2016). The hydrochemistry is characterised by oxidising redox conditions (Newsome et al., 2014), near neutral pH (6.5 ± 1.0) and generally low ionic strength groundwater ($4 \pm 2 \times 10^{-3}$ mol L^{-1}) dominated by Na^+, Ca^{2+}, Cl^- and HCO_3^- ions (Robinson et al., 2023).

Samples were stored in woven polypropylene bags at 4 °C. Representative subsamples for use in sorption experiments (approximately 500 g) were produced by cone and quartering. These subsamples were cation exchanged with a 0.1 mol L^{-1} NaCl solution (100 g L^{-1}) and washed with deionised water (DIW) until the supernatant conductivity was <10 μS cm^{-1} to produce sediments with cation exchange sites uniformly saturated with Na^+ ions. Finally, sediments were oven dried at 102 °C prior to use in batch sorption experiments.

2.2. Sediment characterisation

Particle size distribution (PSD) was determined using British Standard method (BS ISO 11277:2020). Each sample was sieved using apertures 2–22.4 mm. Wet sieve analysis and sedimentation (based off Stokes Law) defined PSD of grainsizes <2 mm by separating agglomerations of sediment. To further determine particle size of <2 mm fraction of samples D and E, further analysis using CAMSIZER X2 (with XJET module) which dispersed <2 mm particles by compressed air. Powder X-ray diffraction (XRD) analysis was performed using Spex ball milled sediment on a Bruker D8 diffractometer. Diffraction patterns were scanned from 2 to 86° 2θ for 1.1 h at a step size of 0.02°, using a Cu tube operated at 40 kV and 40 mA. Samples were prepared as fused glass beads (1 g powder sample: 10 g 66% Li tetraborate/34% Li metaborate flux) and major elemental composition was determined by X-ray fluorescence (XRF) on a Rigaku ZSX Primus II with an Rh tube.

Cation exchange capacity (CEC) was determined for samples (<22.4 mm) in triplicate 50 ml centrifuge tubes using the $BaCl_2$ compulsive exchange method (Gillman and Sumpter, 1986). CEC values (meq 100 g^{-1}) were calculated from the increase in mass (due to formation of $BaSO_4$) following a series of ion exchange reactions. N_2 adsorption Brunauer-Emmett-Teller (BET) surface area was determined for < 5.6 mm oven dried samples that were degassed overnight using N_2 on Micrometrics FlowPrep 060, followed by analysis of specific surface area (SSA_{BET}, m^2 g^{-1}) using Micrometrics Gemini VII 2390. The instrument is not designed to measure SSA_{BET} of > 5.6 mm material.

Reported CEC and SSA_{BET} values were adjusted to account for larger grainsize material excluded from testing. Sediment mass was multiplied by the fraction of the sample incorporated in the experiment to scale CEC values. For example, by assuming that > 22.4 mm grainsizes did not contribute to CEC the scaled value decreased. Sediment > 5.6 mm was similarly scaled using PSDs (Fig. 1), consequently the SSA_{BET} value halved for sample C.

Sediment samples (> 2 mm clasts) were prepared for scanning electron microscopy (SEM) analysis by embedding in epoxy resin blocks, which were cut and polished using diamond pastes and water free lubricants to produce flat surfaces containing cross sections of sediment grains. After carbon coating (20 nm), back scattered electron (BSE) images were collected (working distance 15 mm; 20 keV) using a Tescan VEGA3 XM SEM equipped with an Oxford Instruments X-max 150 SDD Energy dispersive spectrometer controlled by Aztec 3.3 software.

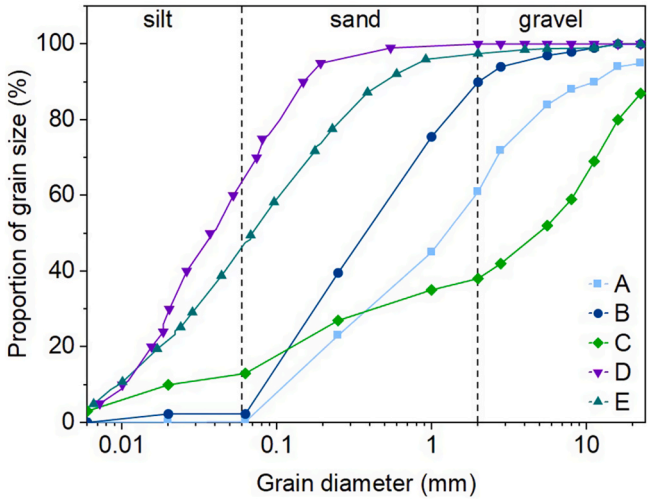

Fig. 1. Cumulative particle size distributions of the unconsolidated aquifer sediment samples used in this study.

2.3. Batch sorption experiments

To investigate the effect of grainsize on adsorption of Sr^{2+}, batch isotherm experiments were conducted at pH 6.5–7.0 and a solid-solution ratio (SSR) of 100 g L^{-1}. This is lower than field conditions (>1000 g L^{-1}) to allow for experimental constraints (Limousin et al., 2007). Strontium solutions were obtained from $SrCl_2.6H_2O$ (Acros Organics) with >99% purity, and all other reagents were analytical grade (>99% purity) chemicals obtained from Fischer Scientific. Aqueous Sr concentrations were analysed by Thermo iCAP 7400 ICP-OES.

Representative sampling and appropriate vessel size for each sample was chosen, as shown in SI Table S1. Stock solutions 0.25 mol L^{-1} NaCl and 0.25 mol L^{-1} $SrCl_2{\cdot}6H_2O$ were prepared and diluted to test adsorption of Sr^{2+} at trace concentrations, ranging from 5.0×10^{-3} to 8.33×10^{-5} mol L^{-1}. A background electrolyte solution containing 2.5×10^{-3} mol L^{-1} NaCl was used in all experiments (this was chosen to replicate the approximate ionic strength found in groundwater samples recovered from the unconsolidated aquifer (McKenzie and Armstrong-Pope, 2010). After equilibrating for 48 h, samples were centrifuged for 10 min, and the pH was monitored with Mettler Toledo InLab 413 SG probe calibrated using pH 4, 7 and 10 buffer solutions. If necessary, pH adjustment to 6.5–7.0 was performed by addition of 10 μL aliquots of 1 mol L^{-1} HCl or 1 mol L^{-1} NaOH. Experiments were then shaken for another 24 h, and the supernatant solution was separated by centrifugation (Table S1). The distribution coefficient (K_d, L kg^{-1}) values were determined using the experimental linear incline of the isotherm, from experiments using Sr^{2+} concentrations from 2.5×10^{-4} mol L^{-1} to 8.3×10^{-4} mol L^{-1}. A higher K_d indicates a greater binding affinity since it describes the ratio between the adsorbed and aqueous species at equilibrium. The K_d was calculated using the following equation (Khan and Khan, 1995):

$$K_d = \frac{Sr_i - Sr_{aq}}{Sr_{aq}} \bullet SSR \quad (1)$$

where Sr_i and Sr_{aq} are initial and equilibrium Sr^{2+} concentrations (mg L^{-1}) and SSR is 100 g L^{-1}. Sorption data from the initial batch isotherm experiment were fitted to the Langmuir isotherm model (Limousin et al., 2007);

$$[Sr]_s = \frac{q_{max} K_L [Sr]_{aq}}{1 + K_L [Sr]_{aq}} \quad (2)$$

where q_{max} defines the maximum adsorption capacity of the sediment and K_L is the Langmuir adsorption constant. R^2 was determined by linear fit of the Langmuir model to experimental data (Langmuir, 1918).

pH dependant adsorption behaviour was also determined using batch sorption tests as above using solutions containing 5.0×10^{-4} mol L^{-1} $SrCl_2$ and 2.5×10^{-3} mol L^{-1} NaCl. Initial pH of the suspensions was set (using 1 mol L^{-1} HCL or 1 mol L^{-1} NaOH) and shaken for 24 h using the experimental conditions outlined in Table S1. After centrifugation, the pH was measured and adjusted to provide solutions ranging from pH 2 to 10.

Batch experiments investigating the effect of increasing ionic strength (IS) on Sr adsorption were prepared with 2.0 mol L^{-1} NaCl stock solution. NaCl background electrolyte ranged from 1.0 mol L^{-1} to 2.5×10^{-3} mol L^{-1} and solutions were spiked with 5.0×10^{-4} mol L^{-1} $SrCl_2$ at pH 6.5–7. The percentage of Sr adsorbed was calculated using the following equation:

$$Sr\ \%\ sorption = \frac{Sr_i - Sr_{aq}}{Sr_i} \bullet 100 \quad (3)$$

where Sr_i and Sr_{aq} are initial and equilibrium Sr concentrations.

2.4. Sorption modelling

The wateq4f.dat database in PHREEQC (USGS) was used to model the effect of pH on grainsize heterogeneity in the experimental solutions (5.0×10^{-4} mol L^{-1} $SrCl_2$, 2.5×10^{-3} mol L^{-1} NaCl) (Parkhurst and Appelo, 1999). Modelling calculations simulated the reaction at pH 2–9 in contact with an ion exchange concentration of sediment derived from the measured CEC (Table 1). The model relied on the competing ion effect of H^+ to simulate the sorption edge for each sample. Surface complexation modelling (SCM) was integrated to better simulate sorption of Sr^{2+} to heterogeneous sediments at pH > 7. The diffuse double layer SCM approach of Dzombak and Morel was applied to simulate sorption of Sr^{2+} to ferrihydrite, using 0.1 x the Fe oxide concentration determined by XRF, to provide the reactive Fe concentration (Dzombak and Morel, 1991). Using sediments relevant to Sellafield, the weak acid extractable Fe was measured to be 2% of the total Fe (Law et al., 2010). This study increased the reactive Fe concentration to 10% to produce a better model fit and account for presence of haematite, which contains amphoteric sites but is not dissolved by weak acid extraction. Sorption of Sr and other divalent cations to variable charge mineral surfaces have been modelled via SCM before (Carroll et al., 2008; Sajih et al., 2014). The study assessed whether the pH sorption edge of heterogeneous sediments could be simulated by a combined ion exchange and SCM approach. To simulate increasing ionic strength, the cation exchange model above was adapted by inclusion of generic ion exchange functions involving Na^+ (Appelo and Postma, 2004).

2.5. Gravel correction experiments

A 0.1 mol L^{-1} NaCl washed subsample from sediment C was prepared by sieving, using 2–22 mm apertures. The Sr^{2+} distribution co-efficient (K_d) for each grainsize fraction (<2, <2.8, <5.6, <8, <11.2, <16, <22.4 mm) was determined using 0.0025 mol L^{-1} NaCl, 0.0005 mol L^{-1} $SrCl_2$ at pH 6.5–7. Sediment was subsampled representatively up to 50 g and shaken at SSR 100 g L^{-1} for 48 h. The following gravel correction equations were applied to the K_d value to compare with the adsorption affinity of the bulk sample. Equations (4) and (5) have been applied to

Table 1
D_{50}, CEC and SSA_{BET} of sediment samples.

Sample	D_{50} (mm)	CEC (meq 100 g^{-1})	SSA_{BET} (m^2 g^{-1})
A	1.2	0.78 ± 0.05	3.73 ± 0.04
B	0.4	1.04 ± 0.02	2.61 ± 0.03
C	5.00	1.24 ± 0.14	1.45 ± 0.03
D	0.04	6.10 ± 0.81	5.28 ± 0.03
E	0.07	5.28 ± 0.62	9.56 ± 0.03

sample C, the heterogeneous gravel.

Equation (4) assumes that all sediment >2 mm is inert and that gravels do not contribute to adsorption. Equation (5) uses a spherical grain assumption and was formulated by measuring K_d values from Hanford gravel sediments in Richland, Washington (Kaplan et al., 2000). In this correction the surface area of the sand, silt and clay fractions are estimated from the PSD and assumes the radius of >2 mm particles are 3 mm. Equation (6) is a surface area gravel correction which quantifies the surface area directly by using SSA_{BET} values. However, BET N_2 analysis technique is unable to measure the SSA_{BET} of particle sizes >5.6 mm.

$$\boldsymbol{K_{d\ gc.inert}} = (\mathbf{1}-\boldsymbol{f})\boldsymbol{K_{d<2mm}} \tag{4}$$

$$\boldsymbol{K_{d\ gc.radii\ est}} = (\mathbf{1}-\boldsymbol{f})\boldsymbol{K_{d<2mm}} + \boldsymbol{f}\left[(\boldsymbol{K_{d<2mm}})\left(\frac{\boldsymbol{r_{<2mm}}}{\boldsymbol{r_{>2mm}}}\right)\right] \tag{5}$$

$$\boldsymbol{K_{d\ gc.BET}} = (\mathbf{1}-\boldsymbol{f})\boldsymbol{K_{d<2mm}} + \boldsymbol{f}\left[(\boldsymbol{K_{d<2mm}})\left(\frac{\boldsymbol{SSA_{>2mm}}}{\boldsymbol{SSA_{<2mm}}}\right)\right] \tag{6}$$

Where f is the gravel fraction (derived from PSD, Fig. 1), r is estimated radius using spherical assumptions for each grainsize and SSA is specific surface area measured by BET N_2 analysis.

3. Results

3.1. Sediment characterisation

Cumulative PSDs (Fig. 1) demonstrates that the five bulk samples collected from Drigg Beach provide sediment with a range of particle sizes and sorting. The mean grain sizes (D_{50}) are reported in Table 1. Samples A and B are characterised as coarse and gravelly sands with respectively 40% and 90% of sediment < 2 mm. Sample C is the most heterogeneous and contains a broad range of grainsize fractions, with 60% > 2 mm. The gravel fractions consist of clasts containing sandstone, other sedimentary rock (such as siltstone) and igneous rock as well as agglomerates. Samples D and E are silt and fine sand (D_{50} 0.04 and 0.07 mm). The clay size fraction was not directly measured using the sedimentation method, but the presence of aluminosilicate clay phases was confirmed by the mineralogical compositions.

XRD analysis showed that the bulk mineralogy of both coarse and fine grained samples are similar (Fig. 2). Quartz is the dominant phase present, along with minor amounts of feldspars (albite and microcline) and aluminosilicate clays (muscovite and clinochlore). The XRD patterns are consistent with other sediment analysis from the area (Law et al., 2010). Samples C and E contained edenite (amphibole group) and calcite, respectively. High SiO_2 content (>70%) in samples is consistent with quartz dominated sediments, and the Al_2O_3 content (7–11 %) is consistent with the aluminosilicates found in XRD analysis. The aquifer sediments contain negligible amounts of organic matter (C_{org} < 0.1 wt %) (Law et al., 2010).

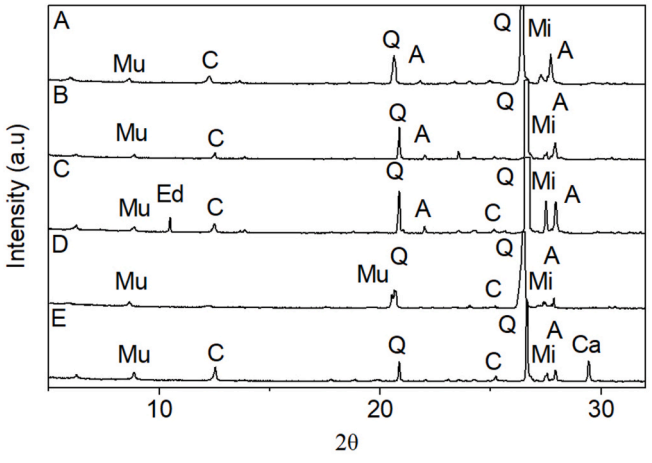

Fig. 2. XRD patterns from bulk sediments. The major quartz peak at 26° 2Θ have been truncated to allow smaller peaks to be discerned. Key: A, albite, $NaAlSi_3O_8$; Ca, calcite, $CaCO_3$; C, clinochlore $(Mg,Al)_6(Si,Al)_4O_{10}(OH)_8$; Mi, microcline, $KAl_2Si_3O_8$; Mu, muscovite $KAl_2Si_3AlO_{10}(OH)_2$; Q, quartz SiO_2; Ed, edenite $NaCa_2Mg_5AlSi_7O_{22}(OH)_2$.

Measured CEC values ranged from 0.8 to 6.1 meq 100 g^{-1}, showing a nearly 8-fold increase between the different grainsize fractions (Table 1). Specific surface area (SSA_{BET}) ranged from 1.45 to 9.6 $m^2\ g^{-1}$, a wider range of surface areas than previously studied from the Sellafield site (2.2–5.9 $m^2\ g^{-1}$) (Newsome et al., 2014). As previously observed, CEC and SSA_{BET} do not correlate precisely with mean particle size (D_{50}). The highest CEC and SSA_{BET} values were recorded in the two fine sand and silt samples (D and E) and the lowest values were determined in the coarse sand sediments (A and B). Sample C (with highest D_{50}) had intermediate CEC, albeit towards the lower end of the range of recorded values and the lowest SSA_{BET} value (1.2 meq 100^{-1} and 1.45 $m^2\ g^{-1}$ respectively).

Low resolution SEM analysis of a sandstone clast recovered from sample C (Fig. 3) revealed a high internal porosity (areas filled with resin appear black in BSE images; porosity was calculated at 35 vol% using ImageJ, SI Figure S2). Electron dispersive spectroscopy (EDS) analysis of the whole field of view (SI Figure S3) showed that the clasts were Si-dominated and also contained Al, Mg, Mo, K, Mn and Fe. This is consistent with a quartz-dominated matrix containing other aluminosillicate phases such as feldspars, clays and Fe oxides. The pore spaces were consistently filled with fine-grained materials. In higher resolution images (Fig. 3f), 20–40 μm crystallites with needle-like cross sections consistent with chlorite were observed in pore spaces (Haile et al., 2015).

3.2. Batch adsorption tests

Sorption isotherms (Fig. 4a) shows a linear K_d relationship up to Sr equilibrium concentration of 25 mg L^{-1}. K_d values (Table 2) shows up to 9-fold increase between the predominantly coarse sand (A and B, 15 and 11 L kg^{-1})) and fine sand and silt samples (D and E, 36 and 96 L kg^{-1}). The well-graded sample (C) has an intermediate K_d (18 L kg^{-1}). At Sr values above 30 mg L^{-1}, Sr sorption is non-linear and fits the Langmuir adsorption model (Fig. 4b shows the linearised version of the Langmuir isotherm with R^2 values ranging from 0.91 to 0.99). The maximum adsorption capacity (q_{max}) is calculated from the isotherm fits (Fig. 4a), which ranges between 1200 and 1400 mg kg^{-1} for samples D and E and 510–300 mg kg^{-1} for the other samples. At high initial Sr values all surfaces were saturated, as expected given the high Sr^{2+} concentrations and optimal pH sorption conditions (pH 6.5–7). Langmuir derived $K_d$values for the fine sand and silt samples are consistent with the linear K_d (D and E, 36 and 112 L kg-1, Table 2). However, K_d values derived from the Langmuir plots overestimate the adsorption for the coarse sands and heterogeneous gravel samples (A, B and C 45, 60 and 80 L kg^{-1}, Table 2.)

3.3. Gravel corrections

The experimental K_d values for sample C grainsize fractions (<2, <2.8, <5.6, <8, <11.2, <16, <22.4 mm) and the corresponding 'gravel corrected' K_d values found using eqns. (4)–(6) are compared to the $K_{d\ (bulk)}$ (18 ± 4 L kg^{-1} (Fig. 5)). The $K_{d(bulk)}$ is an average measured at initial Sr concentration 0.0005 mol L^{-1}; this was compared to the K_d for each sieved grainsize fraction at the same concentration. K_d values determined (with no correction applied) from < 2 mm, < 2.8 and < 5.6 mm sieved fractions overestimate the adsorption of Sr^{2+} to Sample C. As larger grainsizes are incorporated into the sample (from < 8 mm to < 22.4 mm) K_d values (with error bars ± 1 standard deviation) are within error of $K_{d\ (bulk)}$ because of increased inclusion of the larger particles

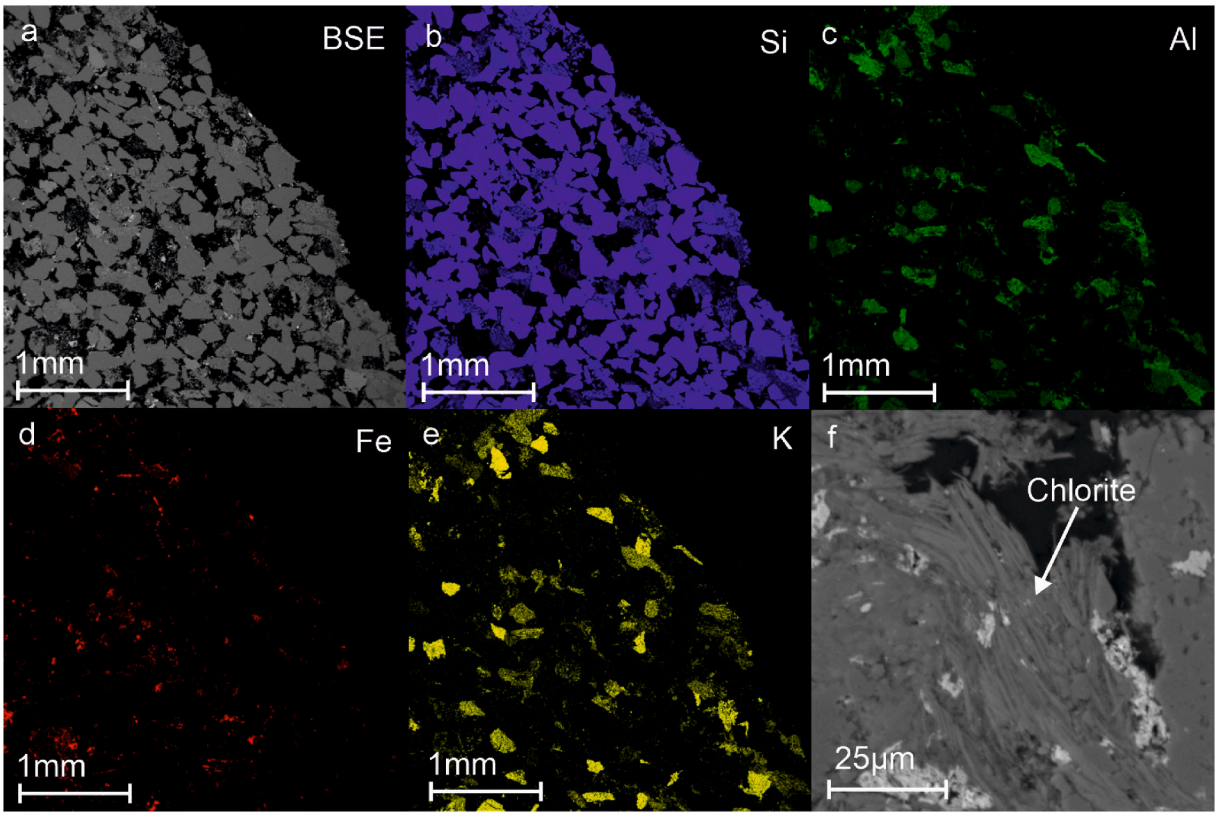

Fig. 3. SEM-EDS analysis of (>2 mm) sandstone clast from sediment sample C; a) low resolution BSE image; b-e) selected false colour element maps; and f) high resolution BSE image of chlorite phase identified in sandstone pore spaces.

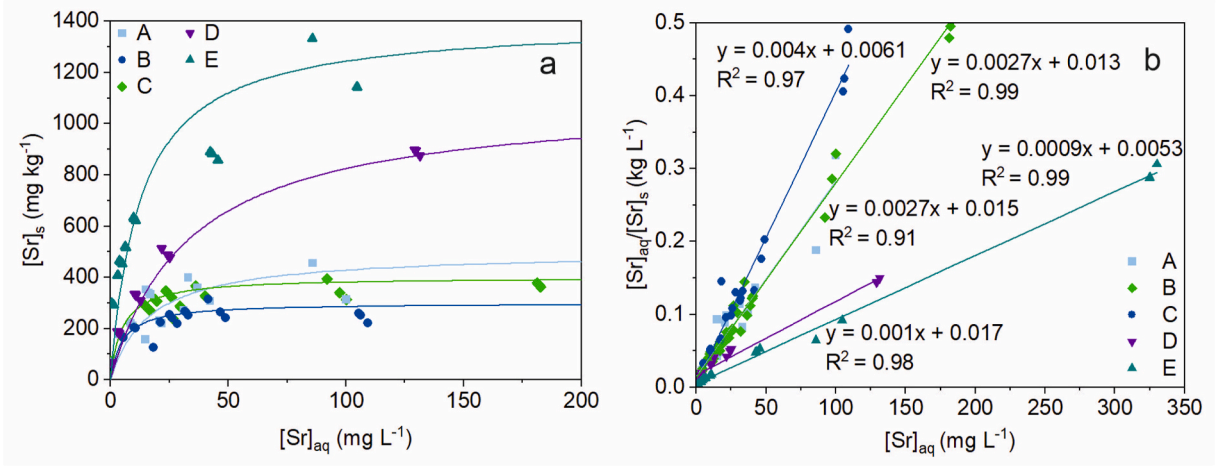

Fig. 4. a) Sr^{2+} sorption to heterogeneous sediments as a function of aqueous [Sr] and best-fit Langmuir adsorption isotherms, and b) linear fits used to calculate isotherm parameters.

present in the bulk sample. This grainsize heterogeneity results in increased standard deviation values, despite using larger sample sizes and masses. K_d calculated using < 8 mm sediment is within error of the $K_{d(bulk)}$ value and is representative of adsorption capacity measured with inclusion of larger grainsizes.

Also shown in Fig. 5 is the efficacy of the various 'gravel correction' approaches (Equation (4)–(6), shown as the symbols without error bars in the lower left side of the plot). The assumption that the surface of > 2 mm particles are inert (Equation (4)) underestimates the $K_{d\ (bulk)}$ value (18 L kg^{-1}). Using SSA_{BET} values in Equation (6) also underestimates $K_{d\ (bulk)}$ and is outside the margin of error. Using the spherical approximation to grainsize provides the closest estimate of the $K_{d\ (bulk)}$.

3.4. pH dependant sorption behaviour

Fig. 6 (shown in more detail in SI Figure S3) demonstrates the effect of grainsize heterogeneity on the pH sorption edge. The highest sorption percentage (93%, Fig. 6a) and K_d (142 L kg^{-1}) was at high pH. Note that the maximum sorption values were calculated from Sr solution concentrations measured close to the limit of detection for Sr^{2+} in analyses, therefore these values represent minimum possible values for these samples. Sorption of Sr^{2+} increases with pH for all grainsizes with a

Table 2
Sr distribution coefficients determined after 48hrs and fitted Langmuir parameters for each of the samples, Langmuir R^2 goodness of fit value calculated from the linearised model ($p < 0.01$, Fig. 4b). K_d values are the mean ± 1σ calculated from Sr^{2+} concentrations <25 mg L^{-1}.

Sample	K_d (L kg^{-1})	Langmuir K_d (L kg^{-1})	q_{max} (mg kg^{-1})	R^2 (linear)	Sample size (n[a])
A	15 ± 7	45.4	510	*0.91*	13
B	11 ± 5	60	300	0.97	15
C	18 ± 6	80	400	0.99	26
D	36 ± 17	36	1200	0.98	9
E	96 ± 27	112	1400	0.99	12

[a] n = number of sorption tests used to define the values given.

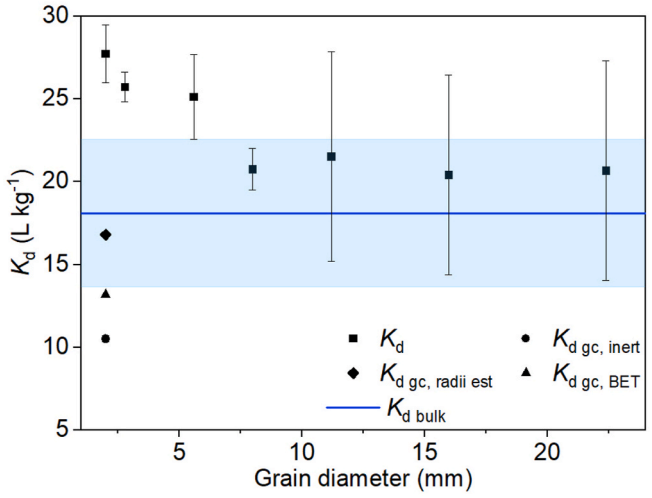

Fig. 5. Effect of increasing sieve cut off size on measured Sr^{2+} K_d for the most heterogeneous sediment sample C, and three gravel corrected K_d values derived from the mean K_d value from the <2 mm fraction using Equations (4)–(6). These are compared to $K_{d\ (bulk)}$ value ± 1σ (shown by shaded area; measured from 8 replicate experiments using [Sr] = 5×10^{-4} mol L^{-1} using bulk sample C material). All data points are the mean of triplicate measurements ± 1σ.

baseline sorption at pH < 3 ranging from 7 to 25%. For fine-sand samples D and E we observe a narrow sorption edge between pH 3–4 with sorption increasing to 80% at pH 5. Sorption to predominantly coarser sand samples A, B and well-graded sample C increases incrementally with pH which provides a broad sorption edge between pH 3–7.

The greatest difference in sorption occurs at low pH where there's a 20-fold difference between K_d values for samples B and E (Figs. 6b, 1 and 20 L kg^{-1}, respectively). As pH increases, the difference in sorption capabilities reduces. At high pH, the variation in sorption between samples reduces to 10%. Sorption behaviour from pH 2–9 was predicted using a combined cation exchange/surface complexation model (SCM) using CEC values that were 50% of the measured value for each sample to empirically fit the analytical model, following the approach used in previous work using similar materials (Wallace et al., 2012). During the model parameterisation, the fitted CEC values used for two pairs of samples were only fractionally different. Therefore, only three solutions are presented to model pH sorption edge for fine, sand and heterogeneous gravel sediments (Figs. 6a and 7a).

Sorption at low pH (2–6) was simulated using solely the cation exchange processes (the surface complexation reaction is only significant at pH > 6). The model simulates the measured data well at circumneutral pH. At low pH, the model overestimates sorption to all grainsize fractions. Inclusion of a combined cation exchange/SCM allows for the increased sorption observed above pH 7 and predicts complete sorption of Sr^{2+} by a combination of both ion exchange and surface complexation reactions at pH 9. The coupled model best simulates pH dependant sorption of Sr^{2+} for samples C and E, and overestimates sorption to samples A and B at pH < 4 by 25%.

3.5. *Ionic strength effect*

The sorption of Sr to the different lithologies/grainsize fractions is plotted in Fig. 7 as a function of increasing ionic strength. Sorption is independent of grainsize at high ionic strength as % sorption converges to 10% for all samples in 1 mol L^{-1} solutions. At lower ionic strength (2.5×10^{-3} - 0.1 mol L^{-1}) there is 30% difference in sorption between the lowest and highest adsorbing sediments (B and E). As ionic strength increases from groundwater to saline conditions, K_d decreases by up to 2 $\log_{10}$ magnitudes (Fig. 7b). The ionic strength effects were predicted using a cation exchange model, which converges and predicts 0% sorption at 1 mol L^{-1}. The model overestimates sorption by 10–30% at 2.5×10^{-3} mol L^{-1} and best simulates behaviour at 0.05–0.1 mol L^{-1}.

4. Discussion

4.1. *Effect of concentration on Sr^{2+} sorption*

Linear Sr^{2+} sorption behaviour in observed with Cumbria Coastal Plain sediments obtained from Drigg Beach in experiments with equilibrium Sr^{2+} concentrations up to 0.28×10^{-3} mol L^{-1} (in a background

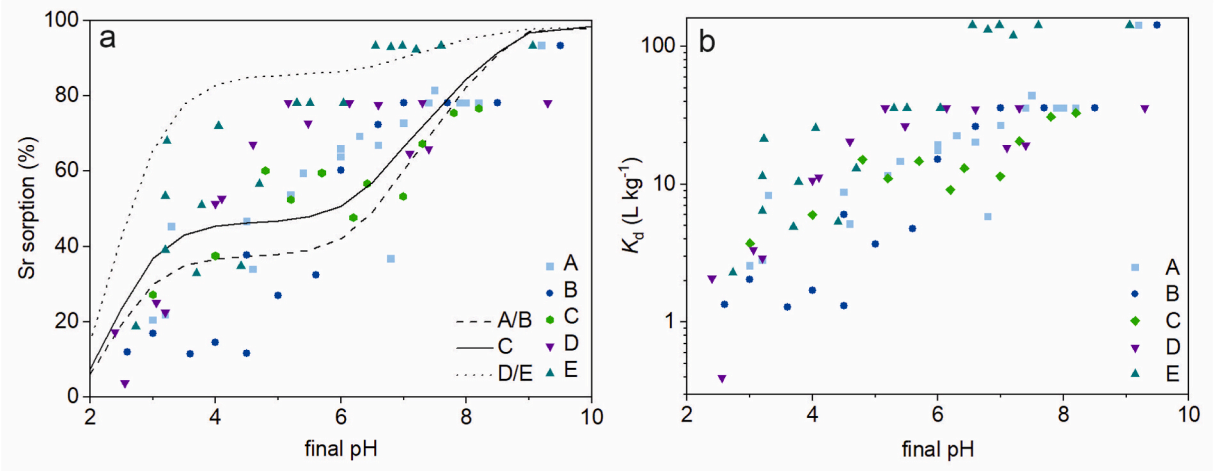

Fig. 6. a) Effect of pH on Sr sorption to different (<22.4 mm) grainsize sediments. Lines show results from coupled cation exchange/surface complexation modelling, b) Effect of pH on Sr^{2+} K_d.

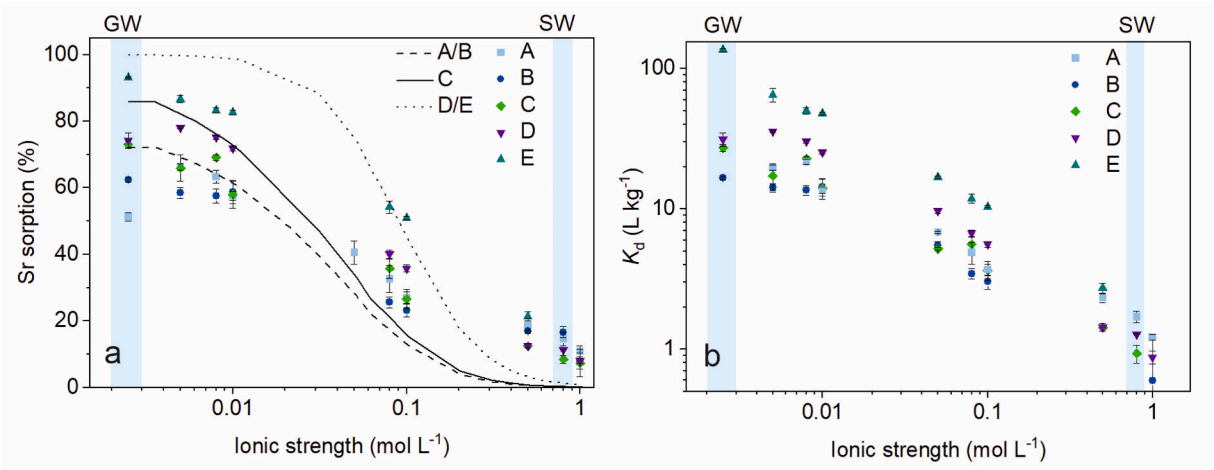

Fig. 7. a) Effect of increasing [Na^+] on Sr^{2+} sorption to <22.4 mm heterogeneous sediments. Lines represent results from cation exchange modelling. b) Effect of increasing [Na^+] on Sr^{2+} K_d values. Groundwater (GW) and seawater (SW) ionic strengths are highlighted in blue.

electrolyte of 2.5×10^{-3} mol L^{-1} Na^+). The typical non-radioactive Sr concentrations in West Cumbrian groundwater is $\sim 0.2 \times 10^{-5}$ mol L^{-1} and the total ionic strength is $\sim 2.5 \times 10^{-3}$ mol L^{-1} (McKenzie and Armstrong-Pope, 2010). Therefore, experimental design for sorption experiments should adopt a maximum Sr^{2+} concentration that is within the linear range. This observation also supports the routine use of non-radioactive Sr in sorption experiments instead of radiotracers, which can be cheaper, safer and less complex to determine in solution.

At higher Sr^{2+} concentrations, sorption was non-linear and conforms to the Langmuir isotherm model where solid concentrations do not increase proportionally with increasing solution concentrations due to saturation of available sorption sites (Foo and Hameed, 2010; Sposito, 1984). The SSA_{BET} values for each of the sediments used correlated with both K_d (Pearson's R = 0.92, $p = < 0.05$); and the maximum Sr loading, q_{max} (Pearson's R = 0.92, $p = < 0.05$), highlighting available surface area as the most important control on Sr^{2+} sorption in these mineralogical very similar sediments. K_d derived from Langmuir plots overestimate adsorption of Sr by coarse sediments (A, B and C) since Langmuir K_d is skewed by results from tests with higher Sr^{2+} concentrations where *qmax* is reached. Langmuir and linear K_d values measured for fine sand and silt sediments are consistent since the higher adsorbing sediment have lower equilibria Sr concentrations, which is representative of the concentration range used to calculate linear K_d values.

4.2. Correlation of Sr^{2+} sorption to sediment composition

The Drigg Beach samples represent a range of similar sediment lithologies with a range of grainsizes. The silt and fine sand samples (D_{50} 0.04 and 0.07 mm) have significantly higher surface areas and Sr^{2+} adsorption potential (as defined by measured K_d values, and Langmuir q_{max}). Sr^{2+} is predicted to adsorb via an outer sphere adsorption mechanism, whereby the cation retains its hydration sphere and forms weak complexes at the solid water interface (Fuller et al., 2016; Thorpe et al., 2012; Vettese et al., 2023). Hence, adsorption increases as grainsize decreases, due to a higher surface area to volume ratio (Limousin et al., 2007).

The coarser sand and gravel sediments (D_{50} 0.4, 1.2 and 5.0 mm) have lower surface area parameters. There is no significant correlation (SI Table S3) between % of particles < 2 mm, CEC and SSA_{BET} measurements ($p > 0.1$). This is partly due to limitations of the methods for measuring heterogeneous sediments, for example BET N_2 gas adsorption technique requires scaling to account for particles with > 5.6 mm grainsizes. However, both K_d and q_{max} values correlate significantly with SSA_{BET} ($p < 0.05$) measured for each sample, and CEC values correlate with q_{max} values ($p < 0.05$). Hence, specific surface area is a good proxy for the total number of Sr^{2+} sorption sites and suggests that cation exchange modelling should be a good approach to predicting ^{90}Sr sorption in contaminated groundwater in these sediment types.

The most well-graded and gravel-rich sediment (sample C) had intermediate K_d, CEC and SSA_{BET} values compared to the fine sand and coarse sand samples. Further evidence of this gravel having an intermediate sorption behaviour is shown in the isotherm data for increasing ionic strength. SEM images and elemental mapping confirmed that clasts within the gravel are comprised of porous sandstone, with clay minerals and iron oxide particles observed in the pore spaces providing additional surface sites for ^{90}Sr sorption. Weathering of feldspars in sandstones to clay minerals (such as chlorite) is known to increase porosity (Blum, 1994; Singer et al., 2014) providing additional sorption surfaces for ^{90}Sr uptake. Other sedimentary (mudstone, siltstone) and igneous clasts are also present, however due to their fine grain sizes and high crystallinity these are not expected to contain accessible porosity or contribute much to Sr^{2+}sorption potential. Therefore, the assumption that sediment > 2 mm is inert is not correct for these sediments and should be considered when applying gravel corrections.

4.3. Use of gravel corrections

To directly determine Sr^{2+} K_d values that are representative of heterogeneous material (which contained gravel particles < 22.4 mm) required that the screening cut-off sieve size was increased from 2 mm (a commonly used size cut-off used in soil and sediment testing; (Krupka et al., 1999; Sposito, 1984)). In this study, using representative sediment subsampling with an 8 mm sieve and using larger sorption vessels (250 ml polycarbonate centrifuge bottles) provided K_d values within error of the unscreened bulk sample, whereas using < 2 mm subsamples overestimated K_d values by ~50%. This is because the < 2 mm fraction is known to be biased to high surface area particles with higher sorption potential (Appelo and Postma, 2004; Langmuir, 1997; Limousin et al., 2007). Increasing the excluded clast size limit from 2 mm to 22 mm results in measured K_d values that converge on bulk sample values. Using a clast-cutoff size is reasonably practicable but has two drawbacks; 1, the appropriate cut-off sieve may need to be determined for each sediment and, 2, K_d values determined using larger grainsize fractions are more variable and have higher relative standard deviations. Therefore, it would be advantageous to use the fine (< 2 mm) sediment fraction, which is analytically simpler and produces much more reproducible results, but also need to be corrected to account for sorption to the gravel fractions present.

Here, three gravel corrections were applied. The assumption that the

> 2 mm fraction was inert (Equation (4)) was assessed and shown to provide an extremely conservative approach to estimating Sr^{2+} K_d values for the bulk sediment, because sandstone clasts within the gravel fraction were highly porous and contained fine grained clays and iron oxides. Gravel corrections based on direct Specific Surface Area (via BET) also underestimated K_d. This was due to an effective maximum grainsize of 5.6 mm for BET analysis, which was insufficient to capture the additional surface area present in larger clasts. The closest estimation of the bulk K_d was calculated using a surface area correction calculated by spherical grain assumptions using PSD data. Therefore, provided PSD data is available, K_d measurements from the < 2 mm fraction of heterogeneous sediments can be adequately corrected to provide useable estimates of Sr^{2+} K_d in the bulk materials. Equation (5) assumes that the average radius of gravel is 3 mm, based off Hanford sediment (Kaplan et al., 2000). Fig. 1 shows that the average radius of gravel for Sample C is 4 mm, this study suggests that other sites should parametrise using PSD to reflect the sample specific mean gravel radius in $r_{< 2mm}/r_{> 2mm}$ of Equation (5).

4.4. pH dependant sorption behaviour

There was a significant difference between the pH dependent sorption behaviour of sediments with grainsizes comprising fine sands and silt, and those comprising mainly coarser sands and gravel. Sr^{2+} sorption at lower pH is predicted to be dominated by adsorption to the clay phases present (which have PZC values between pH 2–4; (Alvarez-Silva et al., 2010; Langmuir, 1997)). Hence fine-sand sized and silt sediments have a narrow adsorption edge between pH 3–4, and relatively constant high % sorption above pH 5. In contrast the predominantly coarser-grained and well-graded sediments have a broad Sr^{2+} sorption edge between pH 3–8, with the increase in sorption > pH 6 attributed to adsorption to iron oxide phases (Axe et al., 1998; Mendez and Hiemstra, 2020; Small et al., 1999; Trivedi and Axe, 1999), which provide additional sorption sites in these relatively clay poor sediments. In terms of the Sr^{2+} K_d values derived from these experiments, it is clear that they are highly pH dependant and are only valid in a narrow range of pH. These sediments all buffer water pH to 6.5–7.0, (which is also typical for groundwater recovered from the UK Sellafield nuclear site (Cruickshank, 2012)), making this pH range the simplest and most reliable data to determine experimentally. However, groundwater pH does vary more widely across UK nuclear sites from slightly alkaline to mildly acidic (Thorpe et al., 2012). Empirical measurement of Sr^{2+} sorption outside a single pH range is impractical for routine characterisation. Although site specific empirical relationships can be adopted (i.e. variation in log K_d is approximately linear between pH 3–8), more commonly modelling approaches are used to predict sorption behaviour (Carroll et al., 2008; Missana et al., 2008; Wissocq et al., 2018) based on sediment properties.

Modelling based on cation exchange simulates Sr^{2+} sorption as a function of pH by considering the exchange of surface bound Sr^{2+} with H^+, as pH changes. The model assumes a homogenous surface with a specified number of sites (derived from the measured sediment CEC) and does not account for the effect of pH on mineral heterogeneity. A better model fit was produced by halving CEC values to account for the difference between the higher potential CEC determined at pH 8.1 in the Ba exchange method and the effective CEC present at lower pH values (Brady, 1984; Pansu, 2006). Cation exchange approaches provide reasonable estimates of the % sorption observed between pH 4–7 and reproduces higher sorption in fine grained sediments and lower sorption in coarser and more heterogeneous sediments. However, the increased sorption observed in the heterogeneous sediments above pH 7 was not reproduced. For these materials, a combined modelling approach was required that included both cation exchange and surface complexation processes. The surface complexation module was parametrised using the sediment Fe_2O_3 content measured by XRF. Here it was assumed that 10% of the total Fe_2O_3 was present as reactive ferric oxides with the same surface properties as ferrihydrite (i.e. number of reactive sites). Inclusion of surface complexation allows for Sr^{2+} sorption to occur on amphoteric sites that become progressively more negatively charged between pH 6 and 9. In coupled cation exchange/surface complexation models for more heterogeneous sediments the proportion of Sr^{2+} predicted to be bound to amphoteric sites increases from ~20% to ~70% between pH 6–9, accounting for the increase in sorption observed for these sediments. Conversely in models of the finer grained sediments, surface complexation reactions were less important and predicted Sr^{2+}sorption to the amphoteric sites only increased from ~5 to ~30% between pH 6–9.

4.5. Ionic strength effects

There was a strong ionic strength effect on Sr^{2+} sorption in all the sediment types used at pH 6.5–7.0. There is a linear relationship between measured log K_d values and log ionic strength that could be used to develop site specific empirical predictions for Sr^{2+} sorption as a function of solution ionic strength in similar sediments. Indeed, in the event of seawater flooding of coastal nuclear sites, inundation with high ionic strength water (~0.8 mol L^{-1}) could potentially result in up to 90% Sr^{2+} remobilisation. Previous research reported that ^{90}Sr associated with < 2 mm fractions from similar sediments rapidly desorbed under saline conditions (Eagling et al., 2013). In the current study, sorption decreased with increasing ionic strength as additional Na^+ ions accumulated on sediment surfaces (Sposito, 1984) and competed with Sr^{2+} for available adsorption sites. Previously a similar ionic strength effect on Sr-sorption was observed using Ca^{2+} (Wallace et al., 2012) but at lower solution concentrations due to the doubly charged Ca^{2+} ion. A cation exchange model was therefore used to simulate the exchange of Sr^{2+} by Na^+ using generic exchange constants (Appelo and Postma, 2004), and parameterised using the sediment CEC values. The model results are broadly in line with the experimental data and reproduces the higher Sr^{2+} sorption observed in homogeneous fine grained sediments compared to coarser grained and more heterogeneous sediments. The model also reproduces the convergence in % Sr^{2+} adsorbed at high ionic strength. However, the model tends to slightly over predict % sorption at low ionic strength (probably related to the use of generic exchange constants), and under predict the amount of sorption at high ionic strength. This may indicate the presence of non-exchangeable sorption sites. In contrast to fully exchangeable outer-sphere sorption to clay minerals, Sr^{2+} sorption to iron oxides is reported to have an inner-sphere component that is unaffected by ionic strength (Langley et al., 2009). Therefore, sorption of Sr^{2+} to iron oxides, as predicted in the coupled cation exchange/surface complexation models used above could account for the small amount of residual Sr sorption observed in all sediment types above 0.5 mol L^{-1} total ionic strength.

5. Conclusions

A linear K_d model could be applied to Sr^{2+} sorption in a range of heterogeneous aquifer sediments tested in batch experiments up to equilibrium Sr concentrations of 0.28×10^{-3} mol L^{-1}. Gravel fractions (where present) contained porous sandstone clasts containing both clays and iron oxides, which are not inert with respect to Sr^{2+} sorption. Therefore, for heterogeneous gravel-containing sediments, bulk K_d could be determined directly in larger scale experiments, but also be estimated from K_d of the < 2 mm fractions, using appropriate gravel corrections based on the sediment PSD. Sr^{2+} sorption was highly pH and ionic strength dependant, with lower sorption occurring in both acidic pH and high ionic strength solutions. The pH and ionic strength effects could be modelled as coupled cation exchange/surface complexation processes that take into account outer-sphere adsorption to clay minerals at pH 3–6 and a variable iron oxides adsorption component at > pH 6. These results show that the reactive transport behaviour of $^{90}Sr^{2+}$ in a range of heterogeneous aquifer sediments can potentially be predicted using existing K_d measurements (that have been made on the < 2 mm

fraction) provided other sediment characterisation data such as the bulk PSD and CEC are also available.

CRediT authorship contribution statement

Georgia R. Barker: Writing – review & editing, Writing – original draft, Visualization, Methodology, Formal analysis, Data curation. **Landis Jared West:** Writing – review & editing, Supervision, Formal analysis, Conceptualization. **James T. Graham:** Writing – review & editing, Supervision, Resources, Conceptualization. **Liam Abrahamsen-Mills:** Formal analysis. **Ian T. Burke:** Writing – review & editing, Supervision, Methodology, Formal analysis, Conceptualization.

Declaration of competing interest

The authors declare that they have no known competing financial interests or personal relationships that could have appeared to influence the work reported in this paper.

Data availability

Data will be made available on request.

Acknowledgements

This work was funded by EPSRC and National Nuclear Laboratory via an industrial CASE doctoral training award to G.R.B. The authors would like to thank Stephen Reid (University of Leeds) for ICP-OES analysis and Lesley Neve (University of Leeds) for XRD and XRF analysis of sediments. Felipe Gallardo Ceron (University of Leeds) is thanked for sharing his CAMSIZER X2 particle size data and Dr Richard Walshaw (University of Leeds) is thanked for his assistance with SEM-EDS analysis.

Appendix A. Supplementary data

Supplementary data to this article can be found online at https://doi.org/10.1016/j.jenvrad.2024.107451.

References

Alvarez-Silva, M., Uribe-Salas, A., Mirnezami, M., Finch, J., 2010. The point of zero charge of phyllosilicate minerals using the Mular–Roberts titration technique. Miner. Eng. 23, 383–389.
Appelo, C.A.J., Postma, D., 2004. Geochemistry, Groundwater and Pollution. CRC press.
Axe, L., Bunker, G.B., Anderson, P.R., Tyson, T.A., 1998. An XAFS analysis of strontium at the hydrous ferric oxide surface. J. Colloid Interface Sci. 199, 44–52.
Beresford, N.A., Scott, E.M., Copplestone, D., 2020. Field effects studies in the Chernobyl exclusion zone: lessons to be learnt. J. Environ. Radioact. 211, 105893.
Blum, A.E., 1994. Feldspars in weathering. Feldspars and Their Reactions, pp. 595–630.
Brady, N., 1984. The Nature and Properties of Soils.
Carroll, S.A., Roberts, S.K., Criscenti, L.J., O'Day, P.A., 2008. Surface complexation model for strontium sorption to amorphous silica and goethite. Geochem. Trans. 9, 1–26.
Chang, S., Um, W., Kim, W.-S., Kim, H., 2018. Effect of seawater intrusion on radioactive strontium (^{90}Sr) sorption and transport at nuclear power plants. Radiochim. Acta 106, 147–160. https://doi.org/10.1515/ract-2016-2724.
Cruickshank, J., 2012. Findings of the Sellafield Contaminated Land & Groundwater Management Project and the Next Steps for the Land Quality Programme. Land Quality Report. Sellafield Ltd.
Dyer, A., Chow, J.K., Umar, I.M., 2000. The uptake of caesium and strontium radioisotopes onto clays. J. Mater. Chem. 10, 2734–2740.
Eagling, J., Worsfold, P.J., Blake, W.H., Keith-Roach, M.J., 2013. Fate of 90Sr and U (VI) in Dounreay sediments following saline inundation and erosion. Chemosphere 92, 911–917.
Foo, K.Y., Hameed, B.H., 2010. Insights into the modeling of adsorption isotherm systems. Chem. Eng. J. 156, 2–10. https://doi.org/10.1016/j.cej.2009.09.013.
Fuller, A.J., Shaw, S., Peacock, C.L., Trivedi, D., Burke, I.T., 2016. EXAFS study of Sr sorption to illite, goethite, chlorite, and mixed sediment under hyperalkaline conditions. Langmuir 32, 2937–2946. https://doi.org/10.1021/acs.langmuir.5b04633.
Gillman, G., Sumpter, E., 1986. Modification to the compulsive exchange method for measuring exchange characteristics of soils. Soil Res. 24, 61–66.
Haile, B.G., Hellevang, H., Aagaard, P., Jahren, J., 2015. Experimental nucleation and growth of smectite and chlorite coatings on clean feldspar and quartz grain surfaces. Mar. Petrol. Geol. 68, 664–674.
Hodkin, D.J., Stewart, D.I., Graham, J.T., Cibin, G., Burke, I.T., 2018. Enhanced crystallographic incorporation of strontium (II) ions into calcite via preferential adsorption at obtuse growth steps. Cryst. Growth Des. 18, 2836–2843.
Kaplan, D.I., Kutnyakov, I.V., Gamerdinger, A.P., Serne, R.J., Parker, K.E., 2000. Gravel-corrected Kd values. Groundwater 38, 851–857.
Khan, S.A., Khan, M.A., 1995. Sorption of strontium on bentonite. Waste Management 15, 641–650.
Krauskopf, K.B., Bird, D.K., 1967. Introduction to Geochemistry. McGraw-Hill, New York.
Krupka, K.M., Kaplan, D., Whelan, G., Serne, R., Mattigod, S., 1999. Understanding variation in partition coefficient, Kd, values. Volume II: review of geochemistry and available Kd values, for cadmium, cesium, chromium, lead, plutonium, radon, strontium, thorium, tritium (3H), and uranium. Environ. Prot. Agency 341, 341.
Kuras, O., Wilkinson, P.B., Meldrum, P.I., Oxby, L.S., Uhlemann, S., Chambers, J.E., Binley, A., Graham, J., Smith, N.T., Atherton, N., 2016. Geoelectrical monitoring of simulated subsurface leakage to support high-hazard nuclear decommissioning at the Sellafield Site, UK. Sci. Total Environ. 566–567, 350–359. https://doi.org/10.1016/j.scitotenv.2016.04.212.
Langley, S., Gault, A.G., Ibrahim, A., Takahashi, Y., Renaud, R., Fortin, D., Clark, I.D., Ferris, F.G., 2009. Sorption of strontium onto bacteriogenic iron oxides. Environmental science & technology 43, 1008–1014.
Langmuir, D., 1997. Aqueous Environmental. Geochemistry Prentice Hall, Upper Saddle River, NJ, p. 600.
Langmuir, I., 1918. The adsorption of gases on plane surfaces of glass, mica and platinum. J. Am. Chem. Soc. 40, 1361–1403.
Law, G.T., Geissler, A., Boothman, C., Burke, I.T., Livens, F.R., Lloyd, J.R., Morris, K., 2010. Role of nitrate in conditioning aquifer sediments for technetium bioreduction. Environmental Science & Technology 44, 150–155.
Limousin, G., Gaudet, J.-P., Charlet, L., Szenknect, S., Barthes, V., Krimissa, M., 2007. Sorption isotherms: a review on physical bases, modeling and measurement. Appl. Geochem. 22, 249–275.
Livens, F., Baxter, M., 1988. Particle size and radionuclide levels in some west Cumbrian soils. Sci. Total Environ. 70, 1–17.
McKenzie, H., Armstrong-Pope, N., 2010. Groundwater Annual Report 2010. Sellafield Ltd.
McKinley, J.P., Zachara, J.M., Smith, S.C., Liu, C., 2007. Cation exchange reactions controlling desorption of 90Sr2+ from coarse-grained contaminated sediments at the Hanford site, Washington. Geochem. Cosmochim. Acta 71, 305–325.
Mendez, J.C., Hiemstra, T., 2020. High and low affinity sites of ferrihydrite for metal ion adsorption: data and modeling of the alkaline-earth ions Be, Mg, Ca, Sr, Ba, and Ra. Geochem. Cosmochim. Acta 286, 289–305.
Missana, T., Garcia-Gutierrez, M., Alonso, U., 2008. Sorption of strontium onto illite/smectite mixed clays. Phys. Chem. Earth, Parts A/B/C 33, S156–S162.
Newsome, L., Morris, K., Trivedi, D., Atherton, N., Lloyd, J.R., 2014. Microbial reduction of uranium (VI) in sediments of different lithologies collected from Sellafield. Appl. Geochem. 51, 55–64.
O'Day, P.A., Newville, M., Neuhoff, P.S., Sahai, N., Carroll, S.A., 2000. X-ray absorption spectroscopy of strontium (II) coordination: I. Static and thermal disorder in crystalline, hydrated, and precipitated solids and in aqueous solution. J. Colloid Interface Sci. 222, 184–197.
Pansu, M., 2006. Handbook of Soil Analysis. Springer.
Parkhurst, D.L., Appelo, C.A.J., 1999. User's guide to PHREEQC (Version 2): a computer program for speciation, batch-reaction, one-dimensional transport, and inverse geochemical calculations (Report No. 99–4259), Water-Resources Investigations Report. https://doi.org/10.3133/wri994259.
Patterson, R.J., Spoel, T., 1981. Laboratory measurements of the strontium distribution coefficient KdSr for sediments from a shallow sand aquifer. Water Resour. Res. 17, 513–520. https://doi.org/10.1029/WR017i003p00513.
Robinson, C., Shaw, S., Lloyd, J.R., Graham, J., Morris, K., 2023. Phosphate (Bio) mineralization remediation of 90Sr-contaminated groundwaters. ACS EST Water 3, 3223–3234. https://doi.org/10.1021/acsestwater.3c00159.
Sajih, M., Bryan, N., Livens, F., Vaughan, D., Descostes, M., Phrommavanh, V., Nos, J., Morris, K., 2014. Adsorption of radium and barium on goethite and ferrihydrite: a kinetic and surface complexation modelling study. Geochem. Cosmochim. Acta 146, 150–163.
Sellafield Ltd, 2016. Groundwater Monitoring at Sellafield: Annual Data Review 2016.
Singer, D.M., Guo, H., Davis, J.A., 2014. U (VI) and Sr (II) batch sorption and diffusion kinetics into mesoporous silica (MCM-41). Chem. Geol. 390, 152–163.
Small, T.D., Warren, L.A., Roden, E.E., Ferris, F.G., 1999. Sorption of strontium by bacteria, Fe (III) oxide, and bacteria− Fe (III) oxide composites. Environmental science & technology 33, 4465–4470.
Smith, N.T., Merritt, J.W., Phillips, E.R., 2023. High-resolution 3D geological modelling of heterogeneity in poorly exposed glacial deposits using sedimentary and glaciotectonic architectural element analysis: a case example from Sellafield in west Cumbria, UK. Q. J. Eng. Geol. Hydrogeol. 56 qjegh2022-022.
Smith, N.T., Shreeve, J., Kuras, O., 2020. Multi-sensor core logging (MSCL) and X-ray computed tomography imaging of borehole core to aid 3D geological modelling of poorly exposed unconsolidated superficial sediments underlying complex industrial sites: an example from Sellafield nuclear site, UK. J. Appl. Geophys. 178, 104084.
Sposito, G., 1984. The Surface Chemistry of Soils. Oxford university press.
Standring, W.J.F., Oughton, D.H., Salbu, B., 2002. Potential remobilization of 137Cs, 60Co, 99Tc, and 90Sr from contaminated Mayak sediments in river and estuary

environments. Environ. Sci. Technol. 36, 2330–2337. https://doi.org/10.1021/es0103187.
Thorpe, C.L., Lloyd, J.R., Law, G.T., Burke, I.T., Shaw, S., Bryan, N.D., Morris, K., 2012. Strontium sorption and precipitation behaviour during bioreduction in nitrate impacted sediments. Chem. Geol. 306, 114–122.
Trivedi, P., Axe, L., 1999. A comparison of strontium sorption to hydrous aluminum, iron, and manganese oxides. J. Colloid Interface Sci. 218, 554–563.
Turkington, G., Gamage, K.A., Graham, J., 2018. Beta detection of strontium-90 and the potential for direct in situ beta detection for nuclear decommissioning applications. Nucl. Instrum. Methods Phys. Res. Sect. A Accel. Spectrom. Detect. Assoc. Equip. 911, 55–65.
Um, W., Serne, R.J., Last, G.V., Glossbrenner, E.T., 2009. The Effect of Gravel Size Fraction on the Distribution Coefficients of Selected Radionuclides Radionuclides. Pacific Northwest National Lab.(PNNL), Richland, WA (United States).
Vettese, G.F., Morris, K., White-Pettigrew, M., Townsend, L.T., Shaw, S., Boothman, C., Lloyd, J.R., 2023. In situ (bio) remediation treatment options for U and Sr contaminated land: a comparison of radionuclide retention and remobilisation. Environ. Sci. J. Integr. Environ. Res.: Advances.
Wallace, S.H., Shaw, S., Morris, K., Small, J.S., Fuller, A.J., Burke, I.T., 2012. Effect of groundwater pH and ionic strength on strontium sorption in aquifer sediments: implications for 90Sr mobility at contaminated nuclear sites. Appl. Geochem. 27, 1482–1491. https://doi.org/10.1016/j.apgeochem.2012.04.007.
Wissocq, A., Beaucaire, C., Latrille, C., 2018. Application of the multi-site ion exchanger model to the sorption of Sr and Cs on natural clayey sandstone. Appl. Geochem. 93, 167–177.